

Strong Field Ionization to Multiple Electronic States in Water

Joseph P. Farrell,¹ Simon Petretti,² Johann Förster,² Brian K. McFarland,¹ Limor S. Spector,¹ Yulian V. Vanne,² Piero Decleva,³ Philip H. Bucksbaum,¹ Alejandro Saenz,² and Markus Gühr^{1,*}

¹Stanford PULSE Institute, SLAC National Accelerator Lab, 2575 Sand Hill Road, Menlo Park California 94025, USA and Departments of Physics and Applied Physics, Stanford University, Stanford California 94305, USA

²AG Moderne Optik, Institut für Physik, Humboldt-Universität zu Berlin, Newtonstraße 15, D-12489 Berlin, Germany

³Dipartimento di Scienze Chimiche, Università di Trieste, Via L. Giorgieri 1, I-34127 Trieste, Italy

(Received 21 March 2011; published 17 August 2011)

High harmonic spectra show that laser-induced strong field ionization of water has a significant contribution from an inner-valence orbital. Our experiment uses the ratio of H₂O and D₂O high harmonic yields to isolate the characteristic nuclear motion of the molecular ionic states. The nuclear motion initiated via ionization of the highest occupied molecular orbital (HOMO) is small and is expected to lead to similar harmonic yields for the two isotopes. In contrast, ionization of the second least bound orbital (HOMO-1) exhibits itself via a strong bending motion which creates a significant isotope effect. We elaborate on this interpretation by solving the time-dependent Schrödinger equation to simulate strong field ionization and high harmonic generation from the water isotopes. We expect that this isotope marking scheme for probing excited ionic states in strong field processes can be generalized to other molecules.

DOI: 10.1103/PhysRevLett.107.083001

PACS numbers: 33.80.Rv, 42.65.Ky

The superposition of several ionic states resulting from strong field ionization of molecules has been observed via high harmonic generation (HHG). Strong field ionization preferentially ionizes the highest occupied molecular orbital (HOMO). This leaves the molecule in the ground ionic state. Rotational or vibrational preexcitation is typically used to discern ionization from inner-valence orbitals and hence the creation of excited ionic states [1–3]. In this Letter, we show that strong field ionization of water can populate several ionic states. This is done *without* vibrational or rotational preexcitation of the sample. The population of ionic states is probed by the recombination step of HHG [4–6]. The excitation of lower lying valence states triggers an electronic wave packet with femtosecond to attosecond time scale dynamics [7], which was demonstrated recently for the case of fine-split ionic states of krypton [8].

To facilitate the observation of ionization from inner-valence orbitals without preexcitation, we compare the high harmonic yields from different isotopes of water. As first understood by Lein and observed by Baker *et al.*, nuclear dynamics occurring between ionization and recombination are mapped onto the harmonic spectrum and can be isolated by using isotope marked molecules [9,10]. Thus, the presence of multiple ionic states in HHG can be determined if the different ionic states launch significantly different nuclear motion.

We now present an intuitive picture of the theory elaborated in [9]. The ionization of the molecular orbital [either HOMO or the second least bound orbital (HOMO-1) in Fig. 1(a)] launches a vibrational wave packet on an ionic potential energy surface in Fig. 1(c) (red and green, respectively). The harmonic light is emitted as the returning electron recombines with the molecular ion.

Photoionization and HHG recombination are inverse processes [11]. The well-known modulation of extreme ultraviolet photoionization cross sections by the Franck-Condon overlap [shown in Fig. 1(b) for H₂O] then requires the HHG recombination cross section to be modulated by the overlap of the ionic state nuclear wave packet and the neutral vibrational ground state. As the ionic state nuclear

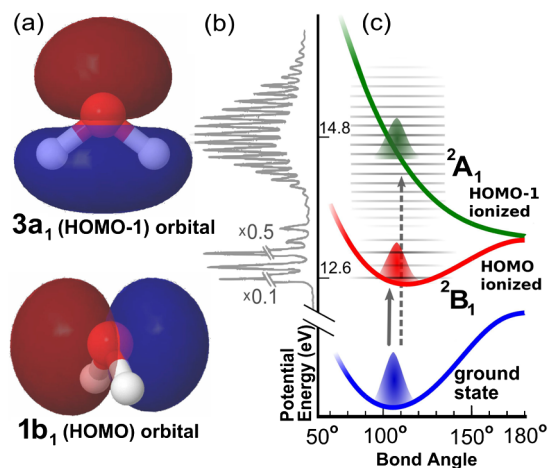


FIG. 1 (color online). (a) Constant amplitude contours of the HOMO ($1b_1$) and HOMO-1 ($3a_1$) orbitals. (b) Photoelectron spectrum of H₂O reproduced from [12]. The transition to the ground ionic state (2B_1 , ionization of HOMO) occurs near 12.6 eV and populates only a few vibrational states. In contrast, the transition to the first excited ionic state (2A_1 , ionization of HOMO-1), which occurs around 14.8 eV, populates many vibrational levels. (c) Potential energy curves of the neutral and first two ionic states. The minimum of the 2B_1 surface lies almost directly above that of the neutral, while the minimum of the 2A_1 surface is at 180°.

wave packet moves, it loses overlap with the ground state. The nuclear wave packet for the heavy isotope is slow, thus maintaining a stronger overlap than the lighter, faster isotope. This gives a larger harmonic yield for the heavier isotope. Since different photon energies correspond to different electron recombination times, the time scale of the nuclear motion is mapped onto harmonic photon energy [9,10]. Comparison of harmonic spectra from the different isotopes isolates the effect of nuclear motion, since their electronic structure is identical.

In H_2O , population of different ionic states can launch significantly different vibrational motion. Ionization of the HOMO, $1b_1$, excites the molecule into the ionic ground state, \tilde{X}^2B_1 . The resulting potential energy surface [Fig. 1(c)] is very similar to that of the neutral as can be seen from the exponentially decaying Franck-Condon progression of the \tilde{X}^2B_1 state in the photoelectron spectrum shown in Fig. 1(b). This is due to the nonbonding properties of the $1b_1$ orbital evident by its shape: the $1b_1$ is a single oxygen p orbital that sticks out of the molecular plane [Fig. 1(a)]. In turn, only extremely *weak* nuclear dynamics are induced upon ionization [12,13]. In contrast, ionization of the HOMO-1 $3a_1$, which sends the molecule into the \tilde{A}^2A_1 state, *strongly* excites the bending mode [12,13]. The equilibrium bond angle changes to 180° [Fig. 1(c)]. The $3a_1$ has an intramolecular bonding character; see Fig. 1(a). The photoelectron spectrum illustrates the strong (weak) vibrational excitation upon ionization of the $3a_1$ ($1b_1$) orbital. The vertical binding energies of the $3a_1$ and $1b_1$ orbitals are 14.8 and 12.6 eV, respectively [14].

The very weak vibrational wave packet excited via population of the ionic ground state indicates that HHG from the $1b_1$ should not display a strong isotope effect. This is confirmed by a recent simulation, which considered ionization solely from the $1b_1$ and found a negligible difference between H_2O and D_2O high harmonics for vibrationally unexcited neutral molecules [15].

Several experiments have shown that inner-valence orbitals can contribute significantly to high harmonic yields [1–3,16]. We expect the inner-valence $3a_1$ orbital to contribute to the high harmonics of water. The broad vibrational wave packet launched via ionization of the $3a_1$ orbital causes a rapid decrease in the overlap between the ionic and ground state nuclear wave functions. This results in a reduction of the HHG yield and significant difference between H_2O and D_2O harmonics. Water is therefore an ideal test molecule to determine inner-valence contributions via nuclear motion. Harmonic generation in water has been demonstrated before in both liquid and gas phase samples [17,18].

We generate harmonics with a commercial Ti:sapphire laser (pulse duration 30 fs, pulse energy 100 μJ , central wavelength 800 nm, repetition rate 1 kHz). A 40 cm focal length mirror focuses the beam to a full width at half maximum of about 60 μm . The harmonics between

20 and 70 eV pass through an Al filter (thickness 100 nm) onto a toroidal flat-field grating, which disperses the radiation onto an extreme ultraviolet sensitive CCD camera. The laser is focused into a gas cell which is approximately 0.5 mm thick and has entrance and exit holes of approximate diameter 0.2 mm. A number density of about 10^{17} cm^{-3} (3 mbar) in the sample is obtained by connecting room temperature water and heavy water reservoirs to the cell with a fine-dosing valve. The laser intensity is changed by inserting pellicle beam splitters into the beam. An iris placed just upstream of the grating rejects the long trajectory harmonics [19].

Figure 2(a) shows the experimental ratios of heavy water to water spectra for several intensities spanning $1\text{--}2 \times 10^{14} \text{ W/cm}^2$. Ratios calculated using odd harmonic peak height or area had negligible differences. The error bars are dominated by a systematic effect characterized by taking two different data sets at different times. The ratio increases monotonically with photon energy for all intensities. In the range 20–50 eV, the ratio spans values from 1 to 1.15. Also, changes in intensity did not measurably affect the ratio of any given harmonic, effectively keeping the slope of the curve constant.

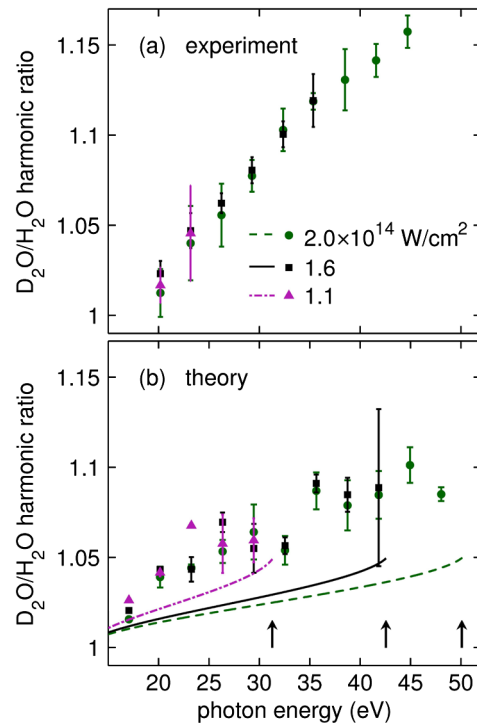


FIG. 2 (color online). (a) Heavy water to water harmonic yield ratios for several intensities. The error bars include the standard error of the mean of the individual data sets, but are dominated by a systematic effect characterized by taking two different sets of spectra at different times. (b) Simulated ratios. Markers represent simulations including both the $1b_1$ and $3a_1$ orbitals for several intensities. Lines represent simulations that solely include the $1b_1$. The classical cutoffs are indicated by arrows. See text for description of the theoretical error bars.

These results show that the D₂O/H₂O harmonic ratio gets progressively larger for longer electron travel times. Thus, strong field ionization launches significant and fast nuclear motion in water. As discussed above, the photoionization studies as well as the disagreement with the 1*b*₁-based simulation in [15] suggest that ionization of the 3*a*₁ is the dominant source of this motion.

To model the experiment, we solve the three-dimensional time-dependent Schrödinger equation (TDSE) in the single-active-electron approximation (SAE) with fixed nuclei separately for each orbital using realistic molecular core potentials. In contrast to [15], based on the three-step model [5], our SAE-TDSE model contains all relative phases between ionization, propagation, and recombination intrinsically, and every step automatically includes the interaction of the active electron with both the molecular core and the laser field. Our approach has been used successfully for H₂ [20] as well as N₂, O₂, and CO₂ [21]. The resulting electronic spectrum is then multiplied by the nuclear autocorrelation function to include the nuclear motion.

We now briefly outline this theoretical method; for details see Refs. [20,21]. Field-free Kohn-Sham orbitals are obtained using the LB94 exchange-correlation potential [22]. They are expressed in a multicentered basis [23], which consists of a set of (typically atom-centered) local spheres (bases) defined as the product of spherical harmonics and a radial part expressed in *B* splines. Molecular symmetry (for water *C*_{2*v*}) is accounted for by implicitly generating equivalent local basis sets at symmetry-equivalent positions. A large central sphere positioned at the charge center of the molecule defines an additional large *B*-spline basis. It overlaps with all atomic-centered spheres and serves for an improved description of the chemical bonding and the molecular electronic continuum. The latter is discretized with a density determined by the size of the central sphere. The radius of the central sphere is set to $r_{\max}^0 = 121.5$ a.u., the maximum number of angular momenta used is $l_{\max} = 12$, and the experimentally determined equilibrium geometry ($R_{\text{OH}} = 0.958$ Å, $\angle\text{HOH} = 104.5^\circ$ [24]) is applied. The time-dependent electronic wave function $|\Psi_\alpha(t)\rangle$ is represented as the sum of the Kohn-Sham orbitals multiplied by time-dependent coefficients. The index α refers to the orbital that is initially occupied. All Kohn-Sham orbitals are propagated in the velocity gauge during their interaction with a 10 cycle \cos^2 laser pulse centered at 800 nm. The HHG spectrum for a single molecular orientation is then

$$\vec{S}_\alpha(\omega) = \left| \int_{-\infty}^{+\infty} dt e^{i\omega t} \omega \vec{d}_\alpha(t) f(t) \right|^2, \quad (1)$$

where $\vec{d}_\alpha(t) = \langle \Psi_\alpha(t) | \vec{p} + \vec{A}(t) | \Psi_\alpha(t) \rangle$. The canonical momentum \vec{p} and the vector potential $\vec{A}(t)$ are expressed in a.u. The damping function $f(t)$ reduces $\vec{d}_\alpha(t)$ at the extreme times to minimize edge effects in the Fourier transform.

We model the isotropic sample by averaging simulated spectra from many different angles between the molecular plane and the laser polarization. This is performed for each orbital separately. Both coherent and incoherent angular averaging give essentially the same ratio D₂O/H₂O. Averaging over only the three main axes of water (including the main ionization axes for the HOMO, HOMO-1, and HOMO-2) approximates very well the ratio obtained with about 80 orientations, equally distributed over the relevant quarter of the unit sphere. Following Lein [9], the influence of nuclear dynamics is included only by the autocorrelation function $C_\alpha(t)$ defined as

$$C_\alpha(t) = \langle \phi_\alpha(0) | \phi_\alpha^+(t) \rangle, \quad (2)$$

where $|\phi_\alpha\rangle$ denotes the vibrational ground state of H₂O and $|\phi_\alpha^+\rangle$ denotes the time-dependent nuclear wave packet launched on H₂O⁺. The autocorrelation functions include all vibrations and are taken from the experiment of Reutt *et al.* [13]. Finally, for each isotope, we form the incoherent sum of the orientation-averaged HHG intensities, $S_{\text{tot}}(\omega)$, from the HOMO $S_{1b_1}(\omega)$ and the HOMO-1 $S_{3a_1}(\omega)$ (the HHG contribution of the HOMO-2 1*b*₂ is found to be negligible) multiplied by the respective autocorrelation functions

$$S_{\text{tot}}(\omega) = \sum_{\alpha=1b_1,3a_1} |C_\alpha(\omega)|^2 S_\alpha(\omega), \quad (3)$$

where we map the time of the autocorrelation function to energy by using Eq. (12) in [9]. This restricts the spectrum to energies below the cutoff. The ratio D₂O/H₂O is then obtained by $S_{\text{tot}}^{(\text{D}_2\text{O})}(\omega)/S_{\text{tot}}^{(\text{H}_2\text{O})}(\omega)$.

The theoretical results are robust with respect to changes in damping function, local peak structure, and the choice of peak height or area. This is reflected in the error bars in Fig. 2(b) which were obtained by systematically varying these parameters.

Figure 2(b) shows simulations using the same intensities as the experiment. In agreement with [15], the isotope effect calculated using only the 1*b*₁ orbital (shown with lines) is very small in comparison to the measurement. The two-orbital simulation (shown with markers) confirms our qualitative estimate that the 3*a*₁ plays an important role. For example, at 45 eV, the experiment, the two-orbital simulation, and the single-orbital simulation have ratios of 1.15, 1.10, and 1.04, respectively.

The intensity dependence of the harmonic spectra is also telling. As stated above, the experimental slope had no discernible dependence on intensity. In contrast, increasing the intensity in the single-orbital simulation decreases the isotope ratio for each harmonic, effectively reducing the slope of the curve. This is expected from the single-orbital picture due to the one-to-one mapping between travel time and photon energy. In agreement with the measurement, the two-orbital simulation does not exhibit a discernible

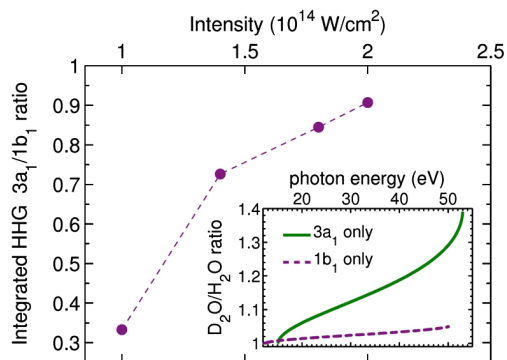


FIG. 3 (color online). Ratio of the calculated total harmonic yields from the $3a_1$ and $1b_1$ orbitals of H_2O as a function of intensity. Inset shows calculated D_2O/H_2O harmonic ratios of the $3a_1$ and $1b_1$ orbitals separately for an intensity of $2 \times 10^{14} \text{ W/cm}^2$.

change in slope with intensity, even though the intensity range used is extremely large.

Examination of the simulations suggests that the independence of the slope on intensity stems from an angular ionization saturation effect. Prior to the laser pulse, the angular probability distribution is isotropic. For a given molecule, the primary ionization direction of the $1b_1$ (perpendicular to the molecular plane) or the $3a_1$ (along the principle axis) are both equally likely to point along the polarization direction of the laser. As the intensity is increased, ionization causes the angular distribution to be depleted along the weakly bound $1b_1$ ionization direction after several cycles of the pulse. The relative weight of HHG from the $3a_1$ then increases with intensity (see Fig. 3). The ratio using only HHG spectra of the $3a_1$ by itself provides an estimate of the upper bound for the isotope effect and is shown in the inset of Fig. 3. A maximum D_2O/H_2O ratio of approximately 1.4 results in this case.

We have shown that population of an excited electronic state can be observed in strong field ionization of gas phase water without using vibrational or rotational preexcitation. Our technique uses isotope marked molecules to isolate the vibrational motion started by ionization. We modeled the multiorbital system by employing a well tested SAE-TDSE simulation framework and show that both the $1b_1$ and $3a_1$ orbitals contribute. The simulation predicts a magnitude of the isotope effect somewhat smaller than is measured but exhibits the same characteristic intensity dependence. The simulation also suggests that the measured independence of the ratio on intensity is due to angular ionization saturation, which increases the relative contribution of the lower valence orbital at high intensities. Finally, our single-orbital simulation predicts a much smaller effect and a different intensity dependence than is measured.

These results provide a new tool for assessing contributions of different orbitals from strong field ionization. In addition, we show that ionization from inner-valence orbitals can also excite nuclear dynamics. This extends the

technique used in [9,10,25] to a larger range of molecules. Possible improvements of the theoretical model include, e.g., an incorporation of the relative phase between the two orbitals [2] and geometry-dependent ionization yields [26].

We thank the Department of Energy, Office of Basic Energy Science, and the Stanford University Dean of Research for support through the Stanford PULSE Institute. We thank COST CM0702 for financial support. S.P. and A.S. acknowledge financial support from the Stifterverband für die Deutsche Wissenschaft, the Fonds der Chemischen Industrie, and Deutsche Forschungsgemeinschaft within SFB 450. L.S.S. acknowledges financial support from NDSEG. P.D. acknowledges financial support from CNR-INFM Democritos and INSTM Crimson. This work was supported in part by the National Science Foundation under Grant No. NSF PHY05-51164.

*Corresponding author.
mguehr@stanford.edu

- [1] B.K. McFarland, J.P. Farrell, P.H. Bucksbaum, and M. Gühr, *Science* **322**, 1232 (2008).
- [2] O. Smirnova *et al.*, *Nature (London)* **460**, 972 (2009).
- [3] W. Li *et al.*, *Science* **322**, 1207 (2008).
- [4] K.C. Kulander, K.J. Schafer, and J.L. Krause, *Laser Phys.* **3**, 359 (1993).
- [5] P.B. Corkum, *Phys. Rev. Lett.* **71**, 1994 (1993).
- [6] K.J. Schafer, B. Yang, L.F. DiMauro, and K.C. Kulander, *Phys. Rev. Lett.* **70**, 1599 (1993).
- [7] Z.-H. Loh *et al.*, *Phys. Rev. Lett.* **98**, 143601 (2007).
- [8] E. Goulielmakis *et al.*, *Nature (London)* **466**, 739 (2010).
- [9] M. Lein, *Phys. Rev. Lett.* **94**, 053004 (2005).
- [10] S. Baker *et al.*, *Science* **312**, 424 (2006); S. Baker *et al.*, *Phys. Rev. Lett.* **101**, 053901 (2008).
- [11] J.P. Farrell *et al.*, *Phys. Rev. A* **83**, 023420 (2011).
- [12] L. Karlsson *et al.*, *J. Chem. Phys.* **62**, 4745 (1975).
- [13] J.E. Reutt, L.S. Wang, Y.T. Lee, and D.A. Shirley, *J. Chem. Phys.* **85**, 6928 (1986).
- [14] C.G. Ning *et al.*, *Chem. Phys.* **343**, 19 (2008).
- [15] M. Falge, V. Engel, and M. Lein, *Phys. Rev. A* **81**, 023412 (2010).
- [16] O. Smirnova *et al.*, *Phys. Rev. Lett.* **102**, 063601 (2009).
- [17] A.D. DiChiara *et al.*, *Opt. Express* **17**, 20959 (2009).
- [18] M.C.H. Wong, J.P. Brichta, and V.R. Bhardwaj, *Opt. Lett.* **35**, 1947 (2010).
- [19] P. Salières, A. L’Huillier, and M. Lewenstein, *Phys. Rev. Lett.* **74**, 3776 (1995).
- [20] M. Awasthi *et al.*, *Phys. Rev. A* **77**, 063403 (2008).
- [21] S. Petretti *et al.*, *Phys. Rev. Lett.* **104**, 223001 (2010).
- [22] R. van Leeuwen and E. J. Baerends, *Phys. Rev. A* **49**, 2421 (1994).
- [23] D. Toffoli, M. Stener, G. Fronzoni, and P. Decleva, *Chem. Phys.* **276**, 25 (2002).
- [24] G. Herzberg, *Molecular Spectra and Molecular Structure III* (Van Nostrand, New York, 1966).
- [25] S. Patchkovskii, *Phys. Rev. Lett.* **102**, 253602 (2009).
- [26] A. Saenz, *J. Phys. B* **33**, 4365 (2000).